frontiers in Materials

ORIGINAL RESEARCH
published: 05 November 2021
doi: 10.3389/fmats.2021.783176

Surface-Functionalized Nanocelluloses as Viscosity-Modifying Agents in Engineered Cementitious Composites

Long Liang[1,2], *Junlei Yang*[3], *Guowei Lv*[3], *Zhen Lei*[3], *Xiurong Li*[2] *and Qiaoling Liu*[1,2,4]*

[1]School of Civil Engineering, Shandong Jianzhu University, Jinan, China, [2]Engineering Research Institute of Appraisal and Strengthening of Shandong Jianzhu University CO., LTD, Jinan, China, [3]Shandong Luqiao Group CO., LTD, Jinan, China, [4]Key Laboratory of Building Structural Retrofitting and Underground Space Engineering of Ministry of Education, Jinan, China

This study investigated the feasibility of using nanofibrilliated celluloses (CNF) (0.1% by weight of binder materials) with three oxidation degrees, no oxidation (NCNF), low oxidation (LCNF), and high oxidation (HCNF), as a viscosity-modifying agent (VMA) to develop polyethylene fiber (PE)-engineered cementitious composites (ECC). Attenuated total reflection-Fourier transform infrared (ATR-FTIR), dynamic light scattering (DLS), and zeta potential were performed to characterize the properties of the CNF with different oxidation degrees. More stable CNF suspensions could be obtained due to the increasing oxidation degree. Rheology tests showed that CNF replacing VMA could modify the plastic viscosity and yield stress of the fresh matrices. With increasing the oxidation degree of CNF, a significant enhancement was seen for the rheological parameters. It was conducted that CNF could increase the compressive strength, the tensile stress, the nominal flexural strength, and the fracture toughness compared with ECC using VMA, and much higher oxidation degrees yielded higher enhancements (HCNF > LCNF > NCNF). ECC using CNF to replace VMA also achieved ultra-high ductility behavior with the tensile strain of over 8% and the saturated multiple cracking pattern. These finds were supplemented by thermal gravimetric analysis (TGA), which showed that the degree of hydration increased with increasing CNF surface oxidation degree. Additionally, the morphology images of PE fibers were observed by scanning electron microscope (SEM).

Keywords: polyethylene fibers, engineered cementitious composites, nanofibrilliated celluloses, rheology, ultra-high ductility, fracture toughness

OPEN ACCESS

Edited by:
Kequan Yu,
Tongji University, China

Reviewed by:
Xiaodan Teng,
Guangxi University, China
Haoliang Wu,
Hong Kong University of Science and Technology, Hong Kong SAR, China

***Correspondence:**
Qiaoling Liu
lql263@163.com

Specialty section:
This article was submitted to Structural Materials, a section of the journal Frontiers in Materials

Received: *25 September 2021*
Accepted: *11 October 2021*
Published: *05 November 2021*

Citation:
Liang L, Yang J, Lv G, Lei Z, Li X and Liu Q (2021) Surface-Functionalized Nanocelluloses as Viscosity-Modifying Agents in Engineered Cementitious Composites. Front. Mater. 8:783176. doi: 10.3389/fmats.2021.783176

INTRODUCTION

Engineered cementitious composites (ECC) are a type of cement-based materials with high ductility, which belongs to the range of fiber-reinforced cementitious composites (FRC). ECC was developed by using binder materials and fine aggregates, mixing with chopped fibers of about 2% volume, and designed according to the theory of fracture mechanics and micromechanics, so as to achieve the high ductility of cement-based materials (Li, 2019). Polyvinyl alcohol (PVA) fibers are used mostly to prepare ECC, which can usually achieve ultimate tensile stress of 3–5 MPa and tensile strain of 1%–5% (Yang et al., 2007; Wu et al., 2018; Zhang et al., 2020). Due to the hydrophilicity of the surface of PVA fibers, a strong chemical bond will be formed between fibers and matrices. When cracks appear under the tensile load, the load is

transferred from PVA fibers to the surrounding matrices, and fibers rupture easily due to the existence of the chemical bond during the debonding process of PVA fibers. The energy generated by the ruptures of fibers is less than that generated by the sliding friction of fibers (Pereira et al., 2012), weakening the bridging ability of PVA fibers, thereby limiting the improvement of the strength and ductility of ECC. Recently, using high-strength and high-elastic modulus polyethylene (PE) fibers to develop ECC has become a hot topic (Yu et al., 2017, 2018; Li et al., 2019). Compared with PVA fibers, the surface of PE fibers is hydrophobic and has higher nominal tensile strength and nominal tensile modulus of elasticity, and then PE fibers embedded in matrices have a higher bridging ability (Wang et al., 2020b), breaking through the limitations of PVA-ECC. The strain-hardening characteristics of ECC are attributed to the bridging effect of fibers, and the uniform dispersion of fibers in matrices is an important prerequisite to achieve this excellent property. The rheological properties of the fresh ECC matrices affect strongly the fiber dispersion uniformity, and it is necessary for combining rheology with ECC micro-design theory to achieve the high ductility of cementitious composites (Li and Li, 2013).

Recently, nanotechnology, an advanced field in science and technology, has been transforming into the field of cement-based materials. Various types of nanomaterials have been applied for improving the mechanical and durability of cement-based materials. Nanofibrilliated celluloses (CNF), as a nature-based resource, are prevailing in reinforcing composite materials (Kang et al., 2018). It is expected to provide a new idea for developing eco-friendly high-performance cement-based materials. CNF is generated by attacking amorphous regions of celluloses (from plant and tree resources), and it has several characteristics such as high aspect ratio, high surface area, low density, and high stiffness compared with other nanomaterials. The properties of CNF composites depend partly on the chemical functionalized surface of CNF (Klemm et al., 2011); a lot of alternate surface chemistries can be obtained due to the difference in the method of degradation, such as sulfate ester, hydroxyl, and acetyl. Additionally, plenty of hydroxyl groups exist on the surface of CNF produced by mechanical methods, and these can be converted to carboxylate groups using TEMPO-mediated oxidation treatments (Xu et al., 2014). On the basis of the surface chemistries of CNF, it is proven that CNF has the ability to modify the rheological properties of cement-based materials (Hisseine et al., 2018a; Montes et al., 2020), and improves the mechanical properties (Hisseine et al., 2018b; Ez-zaki et al., 2021).

Viscosity-modifying agent (VMA) based on cellulose ethers, such as hydroxyethylmethyl cellulose (HEC) or hydroxypropylmethyl cellulose (HPMC), is commonly used to improve the workability and stability of the fresh concrete mixture. In terms of ECC, VMA as an admixture was added to adjust the rheological properties of the fresh matrices for achieving a uniform dispersion of fibers in previous studies (Wang et al., 2020a; Wang et al., 2020b) considering that CNF also can impact the rheological performance of the fresh paste, and it is reported that CNF results in the enhancement of the microstructure and mechanical properties of cement-based materials (Ghahari et al., 2020; Hisseine et al., 2020). In this study, CNF, regarded as an alternative to common VMA, was used to develop and reinforce ECC. The effect of the different surface chemistries, oxidation degrees, of CNF on the performances of ECC was compared. CNF with three oxidation degrees, including no oxidation (NCNF), low oxidation (LCNF), and high oxidation (HCNF), was selected, and the properties of CNF were characterized by attenuated total reflection-Fourier transform infrared (ATR-FTIR), particle size distribution, and zeta potential. A constant CNF content of 0.1% by weight of binder materials was set to produce ECC. The rheological behavior was performed by using the plastic viscosity and yield stress of the fresh ECC matrices, conforming to the Modified Bingham model. A series of mechanical tests consisting of compressive strength, tensile properties, and fracture properties were evaluated at 28 days. In addition, thermal gravimetric analysis (TGA) was conducted to quantify the degrees of hydration of matrices at 28 days.

MATERIALS AND METHODS

Materials

Basic Materials

Ordinary Portland cement (OPC) 52.5 grade, fly ash (FA), and silica fume (SF) were adopted as binder materials, and **Table 1** summarizes their chemical compositions. The quartz sand with a particle size of no more than 0.21 mm was selected as the fine aggregate. The particle size distributions of OPC, FA, SF, and sand are shown in **Figure 1**. Polyethylene (PE) fibers were added to reinforce matrices, and the nominal properties of PE fibers were as follows: the diameter and length were 24 μm and 18 mm, respectively, with a density of 970 kg/m^3. The tensile strength and elastic modulus were 2,900 MPa and 116 GPa, respectively, and the elongation was 2%–3%. Polycarboxylate superplasticizer (SP) was used to adjust the workability of the fresh mixtures. VMA-based hydroxypropylmethylcellulose (HPMC) was introduced to promote the dispersion of fibers.

Surface Functionalized Nanofibrillated Celluloses

Nanofibrillated celluloses (CNFs), extracted from pulps, with different surface oxidation degrees were provided by the Shengquan Group Company, Jinan, China, and they were divided into no oxidation, low oxidation degree, and high oxidation degree. The CNF was a colloidal suspension form with a solid content of 0.6%.

Mixture Proportions and Procedures

The mixture proportions were designed and listed in **Table 2**. Each mixture proportion was named ECC-0.1xCNF, where x represents the oxidation degree, dividing into H (high oxidation degree), L (low oxidation degree), and N (no oxidation). CNF was added to matrices at the same content of 0.1% by the total weight of binder materials. To more uniformly disperse the CNF suspensions in the mortar, they must be homogenized in advance by magnetic stirring and ultrasonic dispersion in water (Cao et al., 2016).

Dry materials including OPC, FA, SF, and sand were mixed for 2 min. For ECC-Ref, water and SP were gradually added into the dry materials and mixed for another 8 min. VMA was needed to add into the fresh matrices and mixed continually

TABLE 1 | Chemical compositions of binder materials (%).

Material	SiO_2	CaO	Al_2O_3	Fe_2O_3	SO_3	MgO	K_2O
Ordinary Portland cement (OPC)	21.2	60.3	3.2	3.98	2.55	1.53	0.75
Fly ash (FA)	53.4	8.12	24.21	4.36	0.45	0.84	1.02
Silica fume (SF)	98.24	0.35	1.52	0.77	—	1.06	1.54

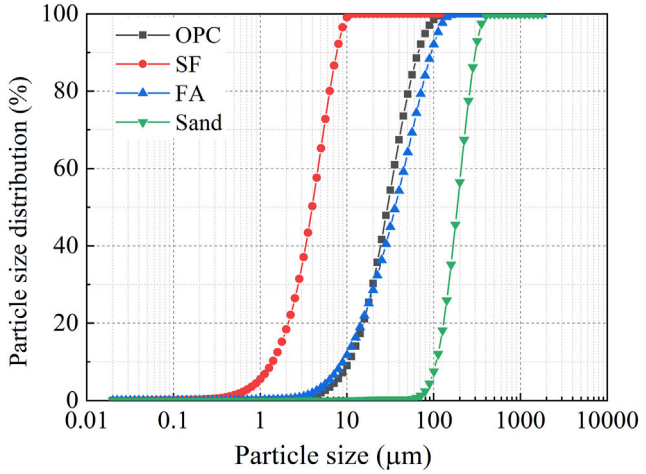

FIGURE 1 | Particle size distribution of ordinary Portland cement (OPC), silica fume (SF), fly ash (FA), and sand.

for 2 min. For ECC-CNF, water, SP, and CNF suspensions were added into the dry materials and mixed for another 8 min. Then, the fresh matrices reached a homogeneous condition. Finally, PE fibers were slowly poured into the mixture, and quickly mixed until fibers were uniformly dispersed. The fresh ECC was cast into molds and demolded after 48 h. All specimens were cured in water at a temperature of 20 ± 2°C until 28 days.

Tests

Attenuated Total Reflection-Fourier Transform Infrared (ATR-FTIR)

CNF suspensions should be dried into a thin film. ATR-FTIR analyses of CNF were conducted using the iS50 FT-IR spectrometer (ThermoFisher Scientific, United States). FTIR spectra were recorded in the wavenumber range of 4,000–450 cm^{-1} with a resolution of 4 cm^{-1} and 32 scans.

Particle Size Distribution and Zeta Potential

Base on the dynamic light scattering (DLS), the particle size distribution and zeta potential were conducted by a zetasizer nano series instrument (Malvern, United Kingdom). The CNF suspensions were dispersed ultrasonically before tests, and the solid content was 0.3%. Then, the sample was analyzed under the following conditions: water refractive index 1.3328, viscosity 0.8827 cP, and temperature 25°C.

Scanning Electron Microscope

SEM was taken to observe the morphology and surface of PE fibers, and samples for SEM were prepared from the fractured section of tensile tests.

Rheology

The rheological properties of the fresh ECC matrices (no fiber) were measured with a rotary rheometer (Kinexus, Malvern, United Kingdom) kept at a constant temperature of 25 ± 0.1°C. A vane spindle with a 25-mm-diameter cup cylinder rheometer was installed (see **Figure 2A**. The fresh matrices were injected into the cup, and a 1-mm gap was set between the spindle and the bottom cup. In the test program from **Figure 2B**, samples went first through pre-shearing to reach the same original state. Then the sample was kept for 30 s to get a stable condition. Finally, the shear rate increased linearly from 0.1 to 100 s^{-1} in 60 s and then decreased linearly to 0.1 s^{-1} in another 60 s.

Thermogravimetric Analysis

TGA was carried out with a TGA/SDTA 851 instrument (Mettler Toledo). Approximately 30 mg of hardened matrices at 28 days were ground into fine powders and heated from 30°C to 1,000°C in a nitrogen atmosphere at a constant rate of 10°C/min.

Compressive Strength

The 28-day compressive strength was measured using 70.7-mm cubes, and the compression tests were conducted on a 3,000-kN servo-hydraulic testing machine under a loading rate of 1 MPa/s.

TABLE 2 | Mixture proportions.

Mixture ID	Binder			Water	Sand	VMA	CNF (%)	SP (%)	Fiber (%)
	OPC	FA	SF						
ECC-Ref	0.5	0.4	0.1	0.22	0.3	0.03%	0	0.4	2
ECC-0.1HCNF	0.5	0.4	0.1	0.22	0.3	0	0.1	0.4	2
ECC-0.1LCNF	0.5	0.4	0.1	0.22	0.3	0	0.1	0.4	2
ECC-0.1NCNF	0.5	0.4	0.1	0.22	0.3	0	0.1	0.4	2

Note: binder, water, and sand are mass fraction; the percentage of viscosity modifying agent (VMA), nanofibrilliated celluloses (CNF), and HRWR is by weight of binder; fiber is by volume of composites.

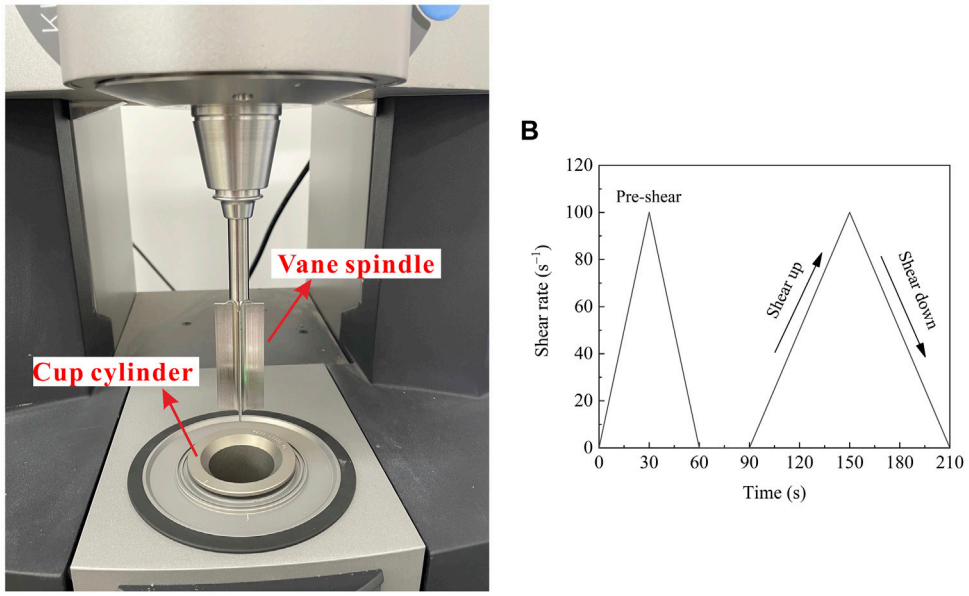

FIGURE 2 | Rheology test. **(A)** Rheometer; **(B)** Test program.

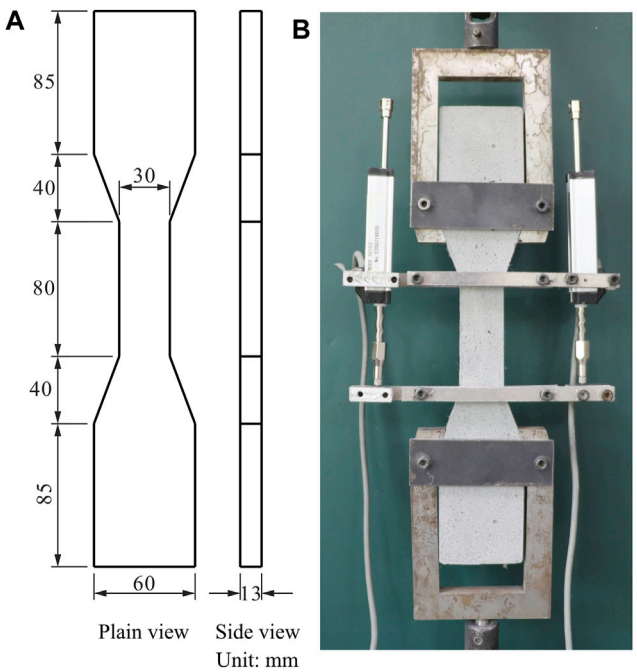

FIGURE 3 | ECC tensile test. **(A)** Dimensions of a dogbone-shaped specimen. **(B)** Test setup.

Tensile Test

The dogbone-shaped specimens were adopted to obtain the uniaxial direct tensile strain–stress curves of ECC (Kanakubo et al., 2005), and the dimensions of the dogbone-shaped specimens and test setup are shown in **Figure 3**. The tensile tests were conducted under a loading rate of 0.5 mm/min. Two extensometers fixed on the middle part with a gauge length of 80 mm were used to measure the elongation of specimens. According to the tensile strain–stress curves, the first cracking stress σtc, ultimate tensile stress σ_{tp}, tensile strain ε_{tu}, crack number n_c, crack width w_c, and crack spacing d_c were obtained to evaluate the tensile properties of ECC.

Fracture Test

According to RILEM TC50-FMC (RILEM, 1985), the prismatic beams of 40 mm × 40 mm × 160 mm were prepared for three-point bending tests. To investigate the fracture effect, a notch with a width of 2 mm and a depth of 10 mm was cut in the middle span of the specimens. The fracture tests were conducted with the span support of 100 mm and a loading rate of 1 mm/min. A clip-gauge was used to measure the crack mouth opening displacement (CMOD). **Figure 4** depicts the test setup and specimen size.

RESULTS

Nanofibrilliated Celluloses Properties

Surface Structure of Nanofibrilliated Celluloses

Figure 5 shows the FTIR spectra of the different CNFs (Li et al., 2015). The band near 3,300 cm^{-1} is assigned to the vibration stretching of O–H from hydroxyl groups. The band at 2,887 cm^{-1} is assigned to the symmetric and asymmetric stretching of C–H from CH_2 groups related to the cellulose structure. The band at 1,590 cm^{-1} is strongly related to the antisymmetric stretching of COO– from carboxylic acid salts, which represents the

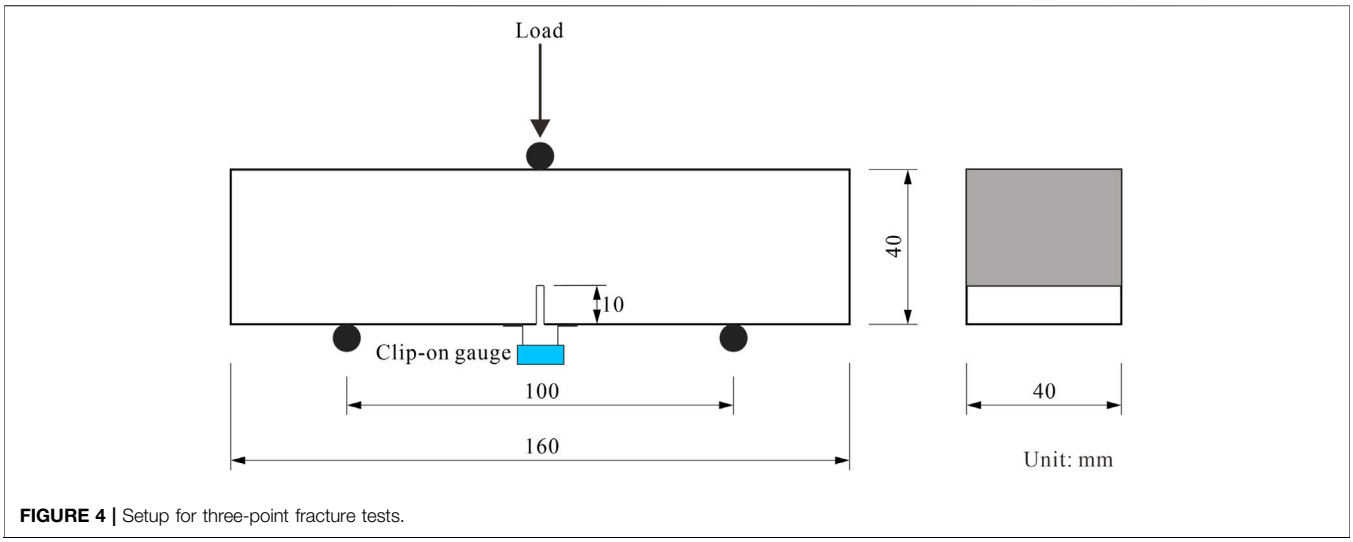

FIGURE 4 | Setup for three-point fracture tests.

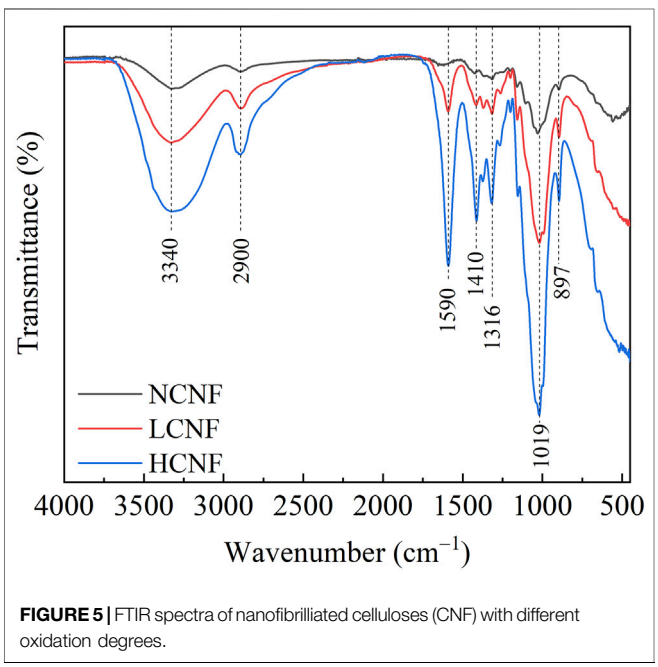

FIGURE 5 | FTIR spectra of nanofibrilliated celluloses (CNF) with different oxidation degrees.

introduction of carboxylate groups oxidized on the surface structure of CNF. HCNF with a higher degree of oxidation had a higher intensity of the COO– band at 1,590 cm^{-1} compared with LCNF, while the peak of NCNF at 1,590 cm^{-1} was absent, which determined the oxidation degree order of HCNF > LCNF > NCNF. Moreover, the hydrophilicity of CNF was determined on the carboxylate and hydroxyl groups.

Particle Size Distribution and Zeta Potential

The dynamic light scattering (DLS) method could quantitatively obtain rough results of the particle size distribution for CNF fibrils (Benini et al., 2018), as shown in **Figure 6A**. It can be seen that the average particle size of CNF gradually decreased from 3,218.49 to 244.78 nm due to the higher oxidation degree. For DLS analysis, the measured particle size is the hydrodynamic diameter of suspensions (Benini et al., 2018), and then aggregated particles might result in a higher value of particle size. Therefore, the decreasing particle size of CNF oxidized might be attributed to the improved dispersion in water. It should be noted that HCNF and LCNF had much lower values of zeta potential (NCNF > LCNF > HCNF), indicating the higher effect of oxidation degree on the stability of CNF suspensions. As shown in **Figure 6B**, after static for 7 days, the HCNF suspension showed high stability, and the LCNF suspension appeared slightly stratified, while NCNF displayed severe precipitation phenomenon, which was ascribed to the surface zeta potential. For the negative value of zeta potential, lower values illustrated that there existed sufficient mutual repulsion, thus, leading to high colloidal stability, and such a similar trend has been reported (Seta et al., 2020).

Rheological Properties of the Fresh Engineered Cementitious Composites Matrices (Constant Superplasticizer)

Figure 7 shows the rheological behavior of the fresh matrices. As can be seen from **Figure 7**, all the fresh matrices exhibited a shear-thinning behavior, showing that the shear viscosity decreased with the increase in shear rate. The yield stress and plastic viscosity were determined by using the Modified Bingham model (expressed in **Eq. 1**) (Yahia and Khayat, 2001) that represents an idealized type of fluid that could fit the shear rate–shear stress curves of cement-based materials, and the fitting results showed quite good correlations with a coefficient of $R^2 > 0.99$.

$$\tau = \tau_0 + \mu\gamma + c\gamma^2 \quad (1)$$

where τ is the shear stress, γ is the shear rate, τ_0 is the yield stress, μ is the plastic viscosity, and c is the regression coefficient.

The fresh matrices for no VMA (with no VMA, no CNF, and 0.4% SP) showed the lowest plastic viscosity and yield

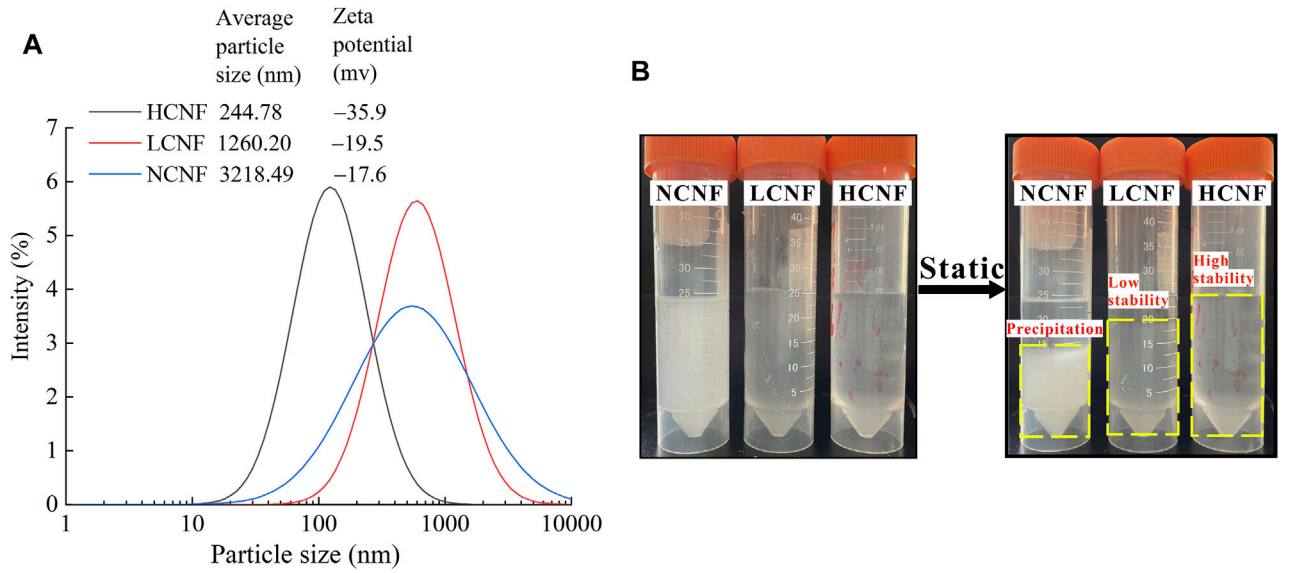

FIGURE 6 | (A) Particle size distribution and zeta potential and **(B)** stability of CNF suspensions.

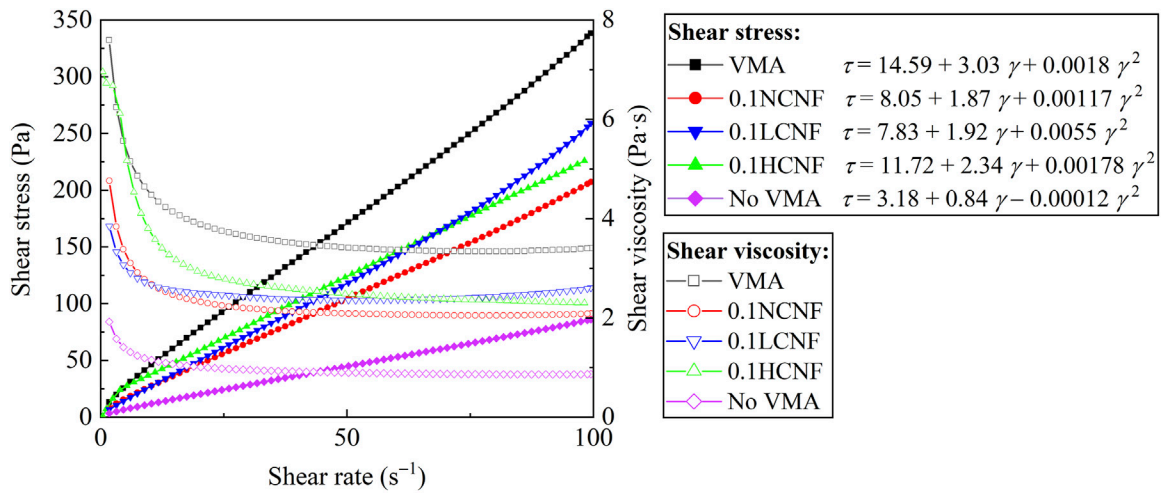

FIGURE 7 | Shear stress and shear viscosity curves of the fresh matrices.

stress of 0.84 Pa·s and 3.18 Pa, respectively. Adding VMA enhanced the plastic viscosity to 3.03 Pa·s by 3.6 times to promote the dispersion of fibers, and the yield stress increased to 14.59 Pa by 4.6 times. In comparison, the incorporation of three types of CNF also increased the plastic viscosity and yield stress to varying degrees. HCNF, LCNF, and NCNF increased the plastic viscosity to 2.34, 1.92, and 1.87 Pa·s, respectively, and these corresponded to increases by 2.8 times, 2.3 times, and 2.2 times, respectively. The yield stress increased to 8.05, 7.83, and 11.70 Pa, respectively, by 2.5 times, 2.5 times, and 3.7 times, respectively. When the CNF content was set to 0.1%, the effect of HCNF on the rheological properties of the fresh matrices was more significant.

The modifying rheological properties mechanism of VMA could be explained as its water retention and adsorption on cement (Pourchez et al., 2006), and that of CNF might be similar. The hydrophilicity of CNF determined its water-absorbed capacity, and HCNF with a higher density of carboxylate groups had more absorbed water. Meanwhile, a lower surface zeta potential of HCNF enhanced the adsorption between CNF and cement, hence, increasing the resistance to deformation of the fresh matrices. Therefore, these results proved the feasibility of using CNF as VMA.

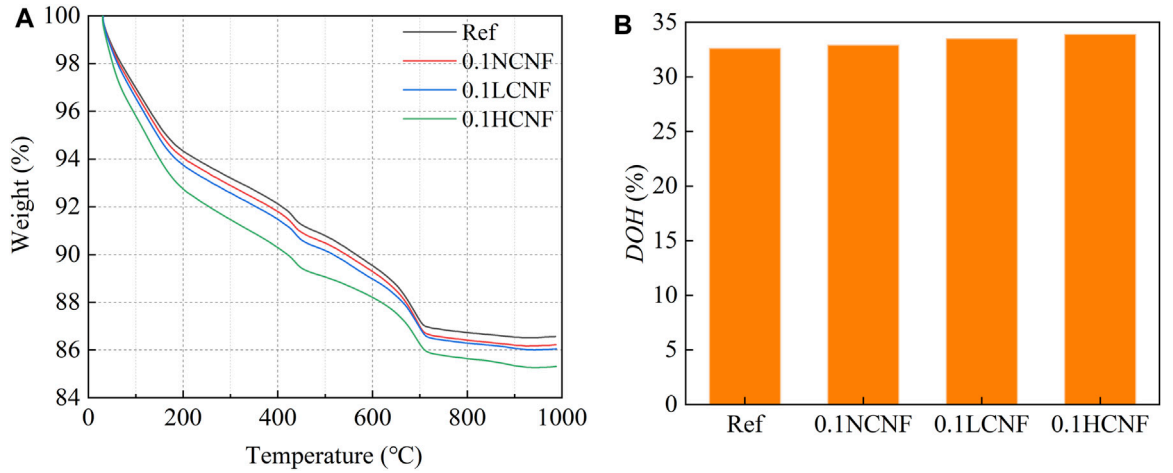

FIGURE 8 | TGA results. **(A)** Weight loss. **(B)** Hydration degree of cement.

Thermogravimetric Analysis

Figure 8A illustrates the thermogravimetric analysis (TGA) results of ECC matrices at 28 days. The weight loss of the non-evaporable water at 105°–1,000°C (Nassiri et al., 2021) could be calculated from the TGA curves. The degree of hydration (DOH) was assessed by normalizing the non-evaporable water content to the assumption maximum hydration value of 0.23 g/g unhydrated cement (Cao et al., 2015), as described by **Eq. 2**.

$$DOH = \frac{W_{NEW}}{0.23}, \quad W_{NEW} = W_{loss} - CO_{loss} \tag{2}$$

where W_{NEW} is the weight loss of non-evaporable water at 105°–1,000°C, W_{loss} is the total weight loss of samples at 105°–1,000°C, and CO_{loss} is the weight loss of decarbonization at 600°–780°C.

The results of DOH are summarized in **Figure 8B**. NCNF, LCNF, and HCNF showed higher DOH than Ref, and the improvement in DOH might be attributed to a short-circuit diffusion mechanism proposed by Cao et al. (2015). The zeta potential for NCNF, LCNF, and HCNF was −17.6 , −19.5, and −35.9 mv, respectively, so CNF had a trend to absorb the surface of cement particles (+1.1 mv). At later ages of hydration, more water might be transported into the unhydrated cement core by the CNF channel, resulting in more hydration products. Meanwhile, HCNF with a higher oxidation degree more strongly tended to adhere to cement particles, thus, giving the highest DOH.

Engineered Cementitious Composite Compressive Strength

Figure 9 shows the results of the 28-day compressive strength. Compared with ECC-Ref for only 60 MPa, CNF with different DOs could always enhance the compressive strength to 65.1, 74.0, and 81.4 MPa, of ECC-0.1NCNF, ECC-0.1LCNF, and ECC-0.1HCNF, respectively, and the peak increase was found in ECC-0.1HCNF by 35.7%, indicating that a higher DO favor an increase in the compressive strength of ECC. The enhancement in the compressive strength of ECC by adding CNF could be due to the acceleration of hydration degrees of cement at 28 days.

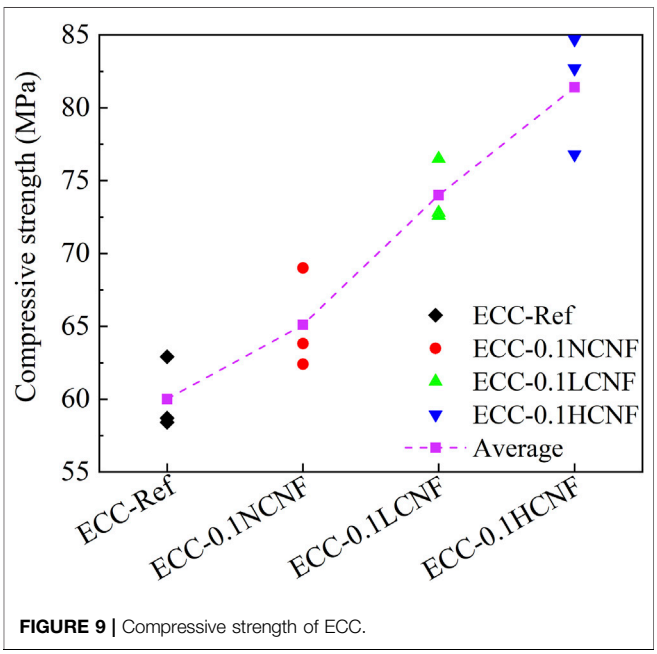

FIGURE 9 | Compressive strength of ECC.

Engineered Cementitious Composite Tensile Properties

Figure 10 illustrates the tensile strain curves of ECC with different types of CNF, and the key tensile parameters are summarized in **Table 3**. It is clearly shown that all specimens exhibited obvious strain-hardening behavior. **Figure 11A** shows the saturated multiple cracking pattern observed in a typical specimens. The tensile strain capacity of all groups could reach over 8%, which was attributed to

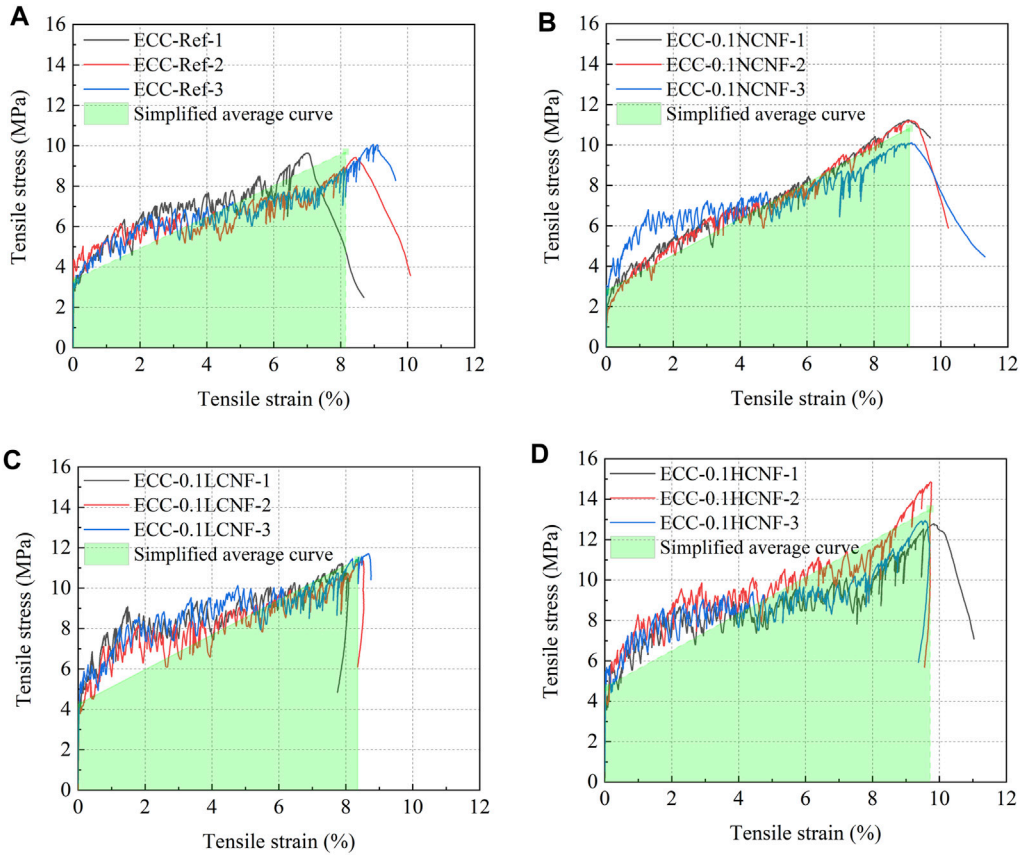

FIGURE 10 | Tensile strain–stress curves of ECC. **(A)** Ref; **(B)** 0.1% content of CNF of no oxidation; **(C)** 0.1% content of CNF of low oxidation degree; **(D)** 0.1% content of CNF of high oxidation degree.

TABLE 3 | Tension test results of engineered cementitious composites (ECC).

Mixture ID	σ_{tc} (MPa)	σ_{tp} (MPa)	ε_{tu} (%)	g_{se} (KJ/m^3)	n_c	w_c (μm)	d_c (mm)
ECC-0CNF	3.37 ± 0.24	9.71 ± 0.27	8.15 ± 0.82	538 ± 51	70 ± 5	107.56 ± 2.60	1.44 ± 0.14
ECC-0.1NCNF	2.79 ± 0.31	10.84 ± 0.53	9.06 ± 0.05	638 ± 14	69 ± 3	120.38 ± 5.62	1.45 ± 0.06
ECC-0.1LCNF	4.25 ± 0.13	11.43 ± 0.20	8.35 ± 0.34	707 ± 37	71 ± 4	111.21 ± 12.11	1.44 ± 0.14
ECC-0.1HCNF	4.70 ± 0.57	13.53 ± 0.94	9.72 ± 0.11	880 ± 43	71 ± 5	131.98 ± 5.10	1.49 ± 0.06

the saturated multiple crack distribution. As shown in **Figure 11B**, during the multiple cracking, the tensile stress dropped when a new crack appeared. Compared with ECC-Ref, the process of strain-hardening behavior for ECC-0.1HCNF was far more fluctuant, and that for ECC-0.1NCNF was more stable.

Figure 12 compares the tensile behavior parameters, the first cracking stress, peak stress, tensile strain, and strain energy, of all groups. As shown in **Figure 12A**, for ECC-Ref, prepared using VMA, the first cracking stress and the peak stress were 3.37 and 9.71 MPa, respectively. Using LCNF and HCNF created a higher first cracking stress and peak stress. HCNF led to 39.5% and 39.3% increases in the first cracking stress of 4.70 MPa and peak stress of 13.53 MPa over those of ECC-Ref, and LCNF led to 26.1% and 17.7% increases in those. NCNF posed a negative effect on the first cracking stress, decreasing by 17.2%, but increased the peak stress by 11.6%. As shown in **Figure 12B**, ECC-Ref, ECC-0.1NCNF, ECC-0.1LCNF, and ECC-0.1HCNF exhibited ultra-high tensile strain capacities of 8.15%, 9.06%, 8.35%, and 9.72%, respectively. In addition, the strain energy dissipation showed a similar trend with the peak stress. ECC prepared using CNF to replace VMA achieved similarly ultra-high ductility. High strength and high ductility are associated with the high bridging capacity provided by the PE fibers and a lower bond between the PE fibers and matrices. On the other hand, when the SP content was set at the same value of 0.4%, the plastic viscosity of the fresh matrices for NCNF, LCNF, and HCNF was 1.87, 1.92, and 2.34 Pa·s, respectively, showing lower values than that for VMA of 3.03 Pa·s. It is

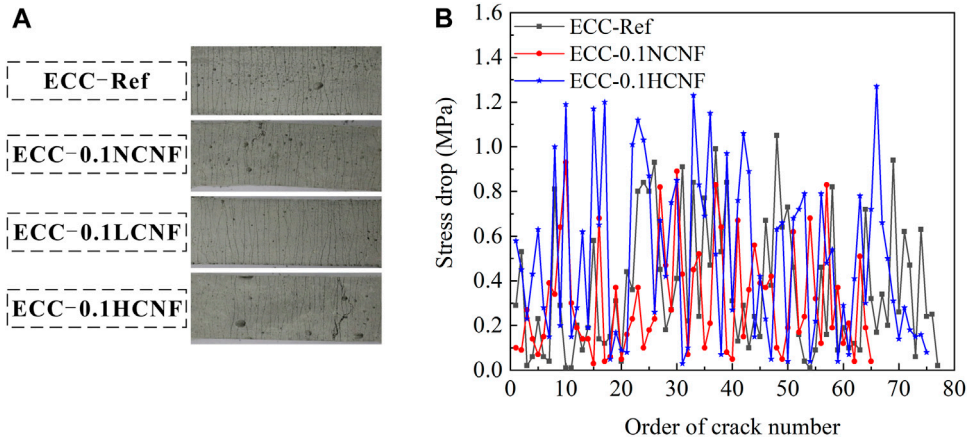

FIGURE 11 | Typical crack patterns of ECC. **(A)** Crack distribution. **(B)** Stress drops.

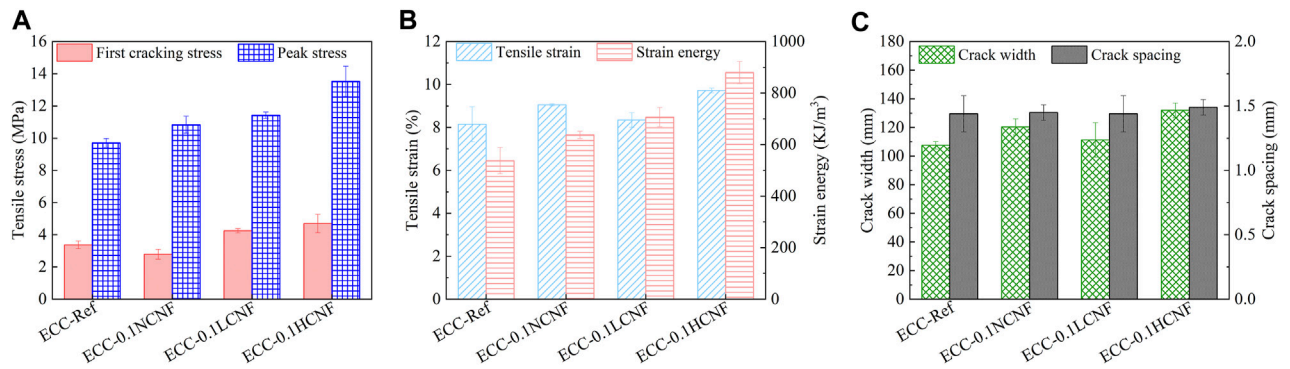

FIGURE 12 | Tensile behavior parameters. **(A)** First cracking stress and peak stress. **(B)** Tensile strain and strain energy. **(C)** Crack width and crack spacing.

noted that the crack number was all close to the value of 70, which caused the differences in the crack width and the crack spacing (see **Figure 12C**). This range for the plastic viscosity all might be suitable for achieving the uniform fiber dispersion. The crack width of ECC introducing CNF was slightly higher than ECC-Ref. The crack width of all specimens was limited to less than 150 μm, exhibiting the excellent ability in the crack width-controlled characteristic (Yu et al., 2017).

Introducing LCNF or HCNF increased the initial cracking stress up to 4.25 MPa for ECC-0.1LCNF and 4.70 MPa for ECC-0.1HCNF and the tensile stress up to 11.43 MPa for ECC-0.1LCNF and 13.53 MPa for ECC-0.1HCNF. These indicated that oxidized CNF exerted a positive effect on the enhancement in the initial cracking stress and tensile stress, and the improvement by 39.5% and 39.3% due to the adding of HCNF was higher than that by 26.1% and 17.7% due to the adding of LCNF.

Engineered Cementitious Composite Fracture Properties

Figure 13 shows the load–CMOD curves of ECC. All groups showed a strong fracture-hardening behavior. In terms of ECC, the nominal flexural strength σ_n is introduced and calculated using **Eq. 3**.

$$\sigma_n = \frac{c_n F_n}{bd} \tag{3}$$

where c_n is the coefficient correlated to the geometric dimensions by **Eq. 4**, and Fn is the peak load.

$$c_n = \frac{3s}{2d\left[1 - (\alpha/d)^2\right]} \tag{4}$$

The ability in the crack resistance can be quantitatively evaluated on the fracture toughness, and the fracture toughness K_{IC} is determined using a simplified method (Xu and Reinhardt, 2000). Based on the load–CMOD curves, the fracture toughness is calculated by **Eq. 5**.

$$K_{IC} = \frac{3F_n s}{2bd^2}\sqrt{a_c} f(V_h) \tag{5}$$

where $f(V_h)$ is the empirical formula for stress factor, as described in **Eq. 6**, and a_c is the critical effective crack length, as shown in **Eq. 7**.

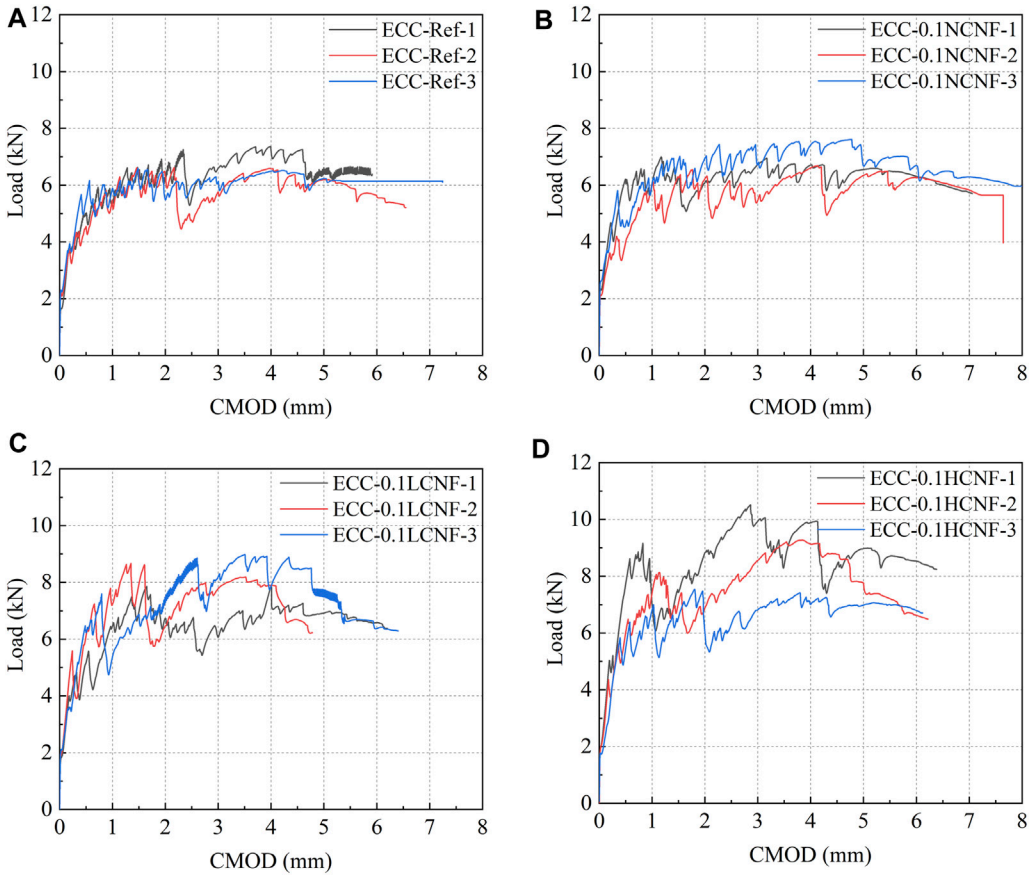

FIGURE 13 | Load–CTOD curves of ECC. **(A)** Ref; **(B)** 0.1% content of CNF of no oxidation; **(C)** 0.1% content of CNF of low oxidation degree; **(D)** 0.1% content of CNF of high oxidation degree.

$$f(V_h) = \frac{1.99 - V_h(1 - V_h)(2.15 - 3.93V_h + 2.7V_h^2)}{(1 + 2V_h)(1 - V_h)^{3/2}}, V_h = \frac{a + h_0}{d + h_0} \tag{6}$$

$$a_c = \frac{2}{\pi}(d + h_0)\arctan\sqrt{\frac{bE \cdot CMOD}{32.6F_n} - 0.1135} - h_0 \tag{7}$$

where E is the elastic modulus and calculated based on the linear elastic stage in the load-CMOD curve, as expressed in **Eq. 8**.

$$E = \frac{F_i}{b \cdot CMOD_i}\left[3.7 + 32.6\tan^2\left(\frac{\pi}{2}V_h\right)\right] \tag{8}$$

Table 4 lists the calculated results of the fracture toughness K_{IC}, the peak load F_n, and fracture energy G_f. Compared with ECC-Ref, it can be observed that the nominal flexural strength for ECC-0.1NCNF, ECC-0.1LCNF, and ECC-0.1HCNF increased by 4.4%, 22.7%, and 34.4%, respectively, which indicated that CNF improved the frictional strength between fibers and matrices. The addition of NCNF, LCNF, and HCNF also enhanced the fracture toughness from 6.03 to 6.30, 7.38, and 8.08 MPa·m$^{1/2}$, respectively, and this corresponded to the enhancements of 4.5%, 20.3%, and 34.0%, respectively. In addition, the fracture-hardening stage of CNF was much larger than that of Ref, thus, leading to the increases in the fracture energy by 4%–27.7%, which was attributed to much stronger PE fiber-bridging capacity. The larger enhancement in the nominal flexural strength, fracture energy, and fracture toughness for ECC-0.1HCNF could be achieved than that for other ECC.

Scanning Electron Microscope Observation of Polyethylene Fibers

Figure 14 displays the morphology images of PE fibers in ECC, including ECC-Ref, ECC-0.1NCNF, and ECC-0.1HCNF. Fibers were embedded and bonded in matrices, contributing to ultra-high tensile strain capacity. It can be observed that most of the fibers were pulled out from matrices, and the hydration products adhered to the surface of the fibers. There was a likely trend in ECC-Ref,

TABLE 4 | Results of fracture parameters of ECC.

Mixture ID	F_n (kN)	σ_n (MPa)	*CMOD* (mm)	G_f (KN·m)	K_{IC} (MPa·m$^{1/2}$)
ECC-0CNF	6.78 ± 0.33	16.95 ± 0.83	4.22 ± 0.27	23.28 ± 0.89	6.03 ± 0.29
ECC-0.1NCNF	7.08 ± 0.39	17.70 ± 0.98	4.03 ± 0.66	24.21 ± 5.29	6.30 ± 0.35
ECC-0.1LCNF	8.32 ± 0.42	20.80 ± 1.05	3.95 ± 0.34	26.65 ± 3.18	7.38 ± 0.37
ECC-0.1HCNF	9.11 ± 1.22	22.78 ± 3.05	4.10 ± 0.17	29.74 ± 3.21	8.08 ± 1.08

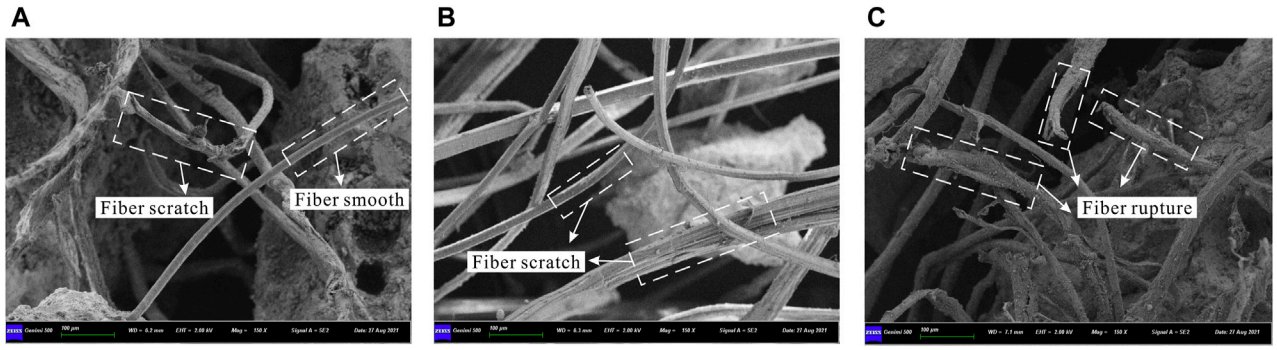

FIGURE 14 | SEM images of polyethylene (PE) fibers in ECC. **(A)** ECC-Ref; **(B)** ECC-0.1NCNF; **(C)** ECC-0.1HCNF.

ECC-0.1NCNF, and ECC-0.1HCNF that the surface of fibers appeared smooth and scratched, and the end of the pulled-out fibers ruptured.

CONCLUSION

This study investigated the feasibility of using CNF as VMA to develop ECC. CNF at 0.1% content with three different oxidation degrees, such as no oxidation, low oxidation degree, and high oxidation degree, namely, NCNF, LCNF, and HCNF, respectively, was used to replace VMA. The micro-scale and macro-scale performances of ECC-Ref, ECC-0.1NCNF, ECC-0.1LCNF, and ECC-0.1HCNF were evaluated. The major conclusions supported that CNF presented a great potential to develop ECC as VMA and reinforcing agent, as follows:

1) Compared with NCNF, LCNF and HCNF with higher surface carboxylate group content had much better stability in water. The high stability of HCNF suspensions was attributed to the higher electrostatic repulsion due to the lower zeta potential.
2) CNF has a significant effect on modifying the rheological properties like VMA. The yield stress and plastic viscosity of the fresh ECC matrices could slightly increase with higher oxidation degrees of CNF, which was traced back to the higher water absorbed capacity of higher carboxylate group contents.
3) NCNF, LCNF, and HCNF increased the cement degree of hydration at 28 days, and the effect of HCNF on the hydration appeared to be higher than that of LCNF and NCNF. HCNF was more easily capable of adhering to the surface of cement particles, becoming the channel to transport more water for the later hydration.
4) CNF with different surface oxidation degrees could effectively improve the mechanical properties compared with ECC-Ref. The compressive strength and the tensile stress increased due to the addition of NCNF, LCNF, and HCNF. The higher oxidation degree of CNF, the greater strength it could increase. The tensile strain capacity for ECC-Ref, ECC-0.1NCNF, ECC-0.1LCNF, and ECC-0.1CNF could all achieve over 8% with the saturated multiple cracking pattern, and the crack widths were all less than 150 μm.
4) The addition of NCNF, LCNF, and HCNF enhanced the fracture properties, including the nominal flexural strength, the fracture energy, and the fracture toughness, and higher enhancements were found with the increasing CNF oxidation degree. This proved that CNF could improve the fiber bridging capacity and the crack resistance of PE fibers.

Although a series of experiments were carried out in the current study, demonstrating the potential of CNF to allow viscosity modifying and nano-reinforcing in ECC, the mechanisms of the reinforced effect still need to be further investigated. Moreover, the long-term performance of CNF in ECC also should be considered in future research.

DATA AVAILABILITY STATEMENT

The original contributions presented in the study are included in the article/Supplementary Material. Further inquiries can be directed to the corresponding author.

AUTHOR CONTRIBUTIONS

Conceptualization, LL and QL; methodology, QL; validation, QL; formal analysis, LL; investigation, JY, GL, and ZL; resources, QL; data curation, LL and XL; writing—original draft preparation, LL and JY; writing—review and editing, QL; supervision, QL; funding acquisition, QL. All authors have read and agreed to the published version of the manuscript.

FUNDING

This research was funded by the National Natural Science Foundation of China (grant nos. 52038006, 52078282, and 51908339), the China Academy of Engineering Consulting Project "Research on Development Strategy and Key Technologies of Bamboo Construction Sector in China towards 2035" (no. 2018-ZCQ-06), and the Program for Changjiang Scholars and Innovative Research Team from the University of China (grant no. IRT_17R69).

REFERENCES

Benini, K. C. C. D. C., Voorwald, H. J. C., Cioffi, M. O. H., Rezende, M. C., and Arantes, V. (2018). Preparation of Nanocellulose from Imperata Brasiliensis Grass Using Taguchi Method. *Carbohydr. Polym.* 192, 337–346. doi:10.1016/j.carbpol.2018.03.055

Cao, Y., Zavaterri, P., Youngblood, J., Moon, R., and Weiss, J. (2015). The Influence of Cellulose Nanocrystal Additions on the Performance of Cement Paste. *Cement and Concrete Composites* 56, 73–83. doi:10.1016/j.cemconcomp.2014.11.008

Cao, Y., Zavattieri, P., Youngblood, J., Moon, R., and Weiss, J. (2016). The Relationship between Cellulose Nanocrystal Dispersion and Strength. *Construction Building Mater.* 119, 71–79. doi:10.1016/j.conbuildmat.2016.03.077

Ez-zaki, H., Riva, L., Bellotto, M., Valentini, L., Garbin, E., Punta, C., et al. (2021). Influence of Cellulose Nanofibrils on the Rheology, Microstructure and Strength of Alkali Activated Ground Granulated Blast-Furnace Slag: a Comparison with Ordinary Portland Cement. *Mater. Struct.* 54, 1–18. doi:10.1617/s11527-020-01614-5

Ghahari, S., Assi, L. N., Alsalman, A., and Alyamaç, K. E. (2020). Fracture Properties Evaluation of Cellulose Nanocrystals Cement Paste. *Materials* 13, 2507. doi:10.3390/ma13112507

Hisseine, O. A., Basic, N., Omran, A. F., and Tagnit-Hamou, A. (2018a). Feasibility of Using Cellulose Filaments as a Viscosity Modifying Agent in Self-Consolidating concrete. *Cement and Concrete Composites* 94, 327–340. doi:10.1016/j.cemconcomp.2018.09.009

Hisseine, O. A., Omran, A. F., and Tagnit-Hamou, A. (2018b). Influence of Cellulose Filaments on Cement Paste and concrete. *J. Mater. Civ. Eng.* 30, 1–14. doi:10.1061/(ASCE)MT.1943-5533.0002287

Hisseine, O. A., Soliman, N. A., Tolnai, B., and Tagnit-Hamou, A. (2020). Nano-engineered Ultra-high Performance concrete for Controlled Autogenous Shrinkage Using Nanocellulose. *Cement Concrete Res.* 137, 106217. doi:10.1016/j.cemconres.2020.106217

Kanakubo, T., Shimizu, K., Katagiri, M., Kanda, T., Fukuyama, H., and Rokugo, K. (2005). Tensile Characteristics Evaluation of DFRCC Round Robin Test Results by JCI-TC. in International RILEM Workshop on High Performance Fiber Reinforced Cementitious Composites in Structural Applications Honolulu, Hawaii: RILEM Publications SARL, 27–36. doi:10.1617/2912143942.004

Kang, X., Kuga, S., Wang, C., Zhao, Y., Wu, M., and Huang, Y. (2018). Green Preparation of Cellulose Nanocrystal and its Application. *ACS Sust. Chem. Eng.* 6, 2954–2960. doi:10.1021/acssuschemeng.7b02363

Klemm, D., Kramer, F., Moritz, S., Lindström, T., Ankerfors, M., Gray, D., et al. (2011). Nanocelluloses: A New Family of Nature-Based Materials. *Angew. Chem. Int. Ed.* 50, 5438–5466. doi:10.1002/anie.201001273

Li, B., Xu, W., Kronlund, D., Määttänen, A., Liu, J., Smått, J.-H., et al. (2015). Cellulose Nanocrystals Prepared via Formic Acid Hydrolysis Followed by TEMPO-Mediated Oxidation. *Carbohydr. Polym.* 133, 605–612. doi:10.1016/j.carbpol.2015.07.033

Li, L., Cai, Z., Yu, K., Zhang, Y. X., and Ding, Y. (2019). Performance-based Design of All-Grade Strain Hardening Cementitious Composites with Compressive Strengths from 40 MPa to 120 MPa. *Cement and Concrete Composites* 97, 202–217. doi:10.1016/j.cemconcomp.2019.01.001

Li, M., and Li, V. C. (2013). Rheology, Fiber Dispersion, and Robust Properties of Engineered Cementitious Composites. *Mater. Struct.* 46, 405–420. doi:10.1617/s11527-012-9909-z

Li, V. C. (2019). *Engineered Cementitious Composites (ECC): Bendable concrete for Sustainable and Resilient Infrastructure*, : SpringerLink. doi:10.1007/978-3-662-58438-5

Montes, F., Fu, T., Youngblood, J. P., and Weiss, J. (2020). Rheological Impact of Using Cellulose Nanocrystals (CNC) in Cement Pastes. *Construction Building Mater.* 235, 117497. doi:10.1016/j.conbuildmat.2019.117497

Nassiri, S., Chen, Z., Jian, G., Zhong, T., Haider, M. M., Li, H., et al. (2021). Comparison of Unique Effects of Two Contrasting Types of Cellulose Nanomaterials on Setting Time, Rheology, and Compressive Strength of Cement Paste. *Cement and Concrete Composites* 123, 104201. doi:10.1016/j.cemconcomp.2021.104201

Pereira, E. B., Fischer, G., and Barros, J. A. O. (2012). Direct Assessment of Tensile Stress-Crack Opening Behavior of Strain Hardening Cementitious Composites (SHCC). *Cement Concrete Res.* 42, 834–846. doi:10.1016/j.cemconres.2012.03.006

Pourchez, J., Peschard, A., Grosseau, P., Guyonnet, R., Guilhot, B., and Vallée, F. (2006). HPMC and HEMC Influence on Cement Hydration. *Cement Concrete Res.* 36, 288–294. doi:10.1016/j.cemconres.2005.08.003

RILEM (1985). Determination of the Fracture Energy of Mortar and concrete by Means of Three-point bend Tests on Notched Beams, *Materials and Struc.* 18, 287–290. doi:10.1007/BF02472918

Seta, F. T., An, X., Liu, L., Zhang, H., Yang, J., Zhang, W., et al. (2020). Preparation and Characterization of High Yield Cellulose Nanocrystals (CNC) Derived from ball Mill Pretreatment and Maleic Acid Hydrolysis. *Carbohydr. Polym.* 234, 115942. doi:10.1016/j.carbpol.2020.115942

Wang, Y., Jian, X., Yu, J., Ye, J., and Dong, F. (2020a). Development of gypsum-based Composites with Tensile Strain-hardening Characteristics. *J. Am. Ceram. Soc.* 103, 7115–7126. doi:10.1111/jace.17419

Wang, Y., Liu, F., Yu, J., Dong, F., and Ye, J. (2020b). Effect of Polyethylene Fiber Content on Physical and Mechanical Properties of Engineered Cementitious Composites. *Construction Building Mater.* 251, 118917. doi:10.1016/j.conbuildmat.2020.118917

Wu, H.-L., Zhang, D., Ellis, B. R., and Li, V. C. (2018). Development of Reactive MgO-Based Engineered Cementitious Composite (ECC) through Accelerated Carbonation Curing. *Construction Building Mater.* 191, 23–31. doi:10.1016/j.conbuildmat.2018.09.196

Xu, Q., Li, W., Cheng, Z., Yang, G., and Qin, M. (2014). TEMPO/NaBr/NaClO-mediated Surface Oxidation of Nanocrystalline Cellulose and its Microparticulate Retention System with Cationic Polyacrylamide. *BioResources* 9, 994–1006. doi:10.15376/biores.9.1.994-1006

Xu, S., and Reinhardt, H. W. (2000). A Simplified Method for Determining Double-K Fracture Parameters for Three-point Bending Tests. *Int. J. Fract.* 104, 181–209. doi:10.1023/A:1007676716549

Yahia, A., and Khayat, K. H. (2001). Analytical Models for Estimating Yield Stress of High-Performance Pseudoplastic Grout. *Cement Concrete Res.* 31, 731–738. doi:10.1016/S0008-8846(01)00476-8

Yang, E. H., Yang, Y., and Li, V. C. (2007). Use of High Volumes of Fly Ash to Improve ECC Mechanical Properties and Material Greenness. *Mj* 104, 620–628. doi:10.14359/18966

Yu, K.-Q., Yu, J.-T., Dai, J.-G., Lu, Z.-D., and Shah, S. P. (2018). Development of Ultra-high Performance Engineered Cementitious Composites Using

Polyethylene (PE) Fibers. *Construction Building Mater.* 158, 217–227. doi:10.1016/j.conbuildmat.2017.10.040

Yu, K., Wang, Y., Yu, J., and Xu, S. (2017). A Strain-Hardening Cementitious Composites with the Tensile Capacity up to 8%. *Constr. Build. Mater.* 137, 410–419. doi:10.1016/j.conbuildmat.2017.01.060

Zhang, D., Jaworska, B., Zhu, H., Dahlquist, K., and Li, V. C. (2020). Engineered Cementitious Composites (ECC) with limestone Calcined clay Cement (LC3). *Cement and Concrete Composites* 114, 103766. doi:10.1016/j.cemconcomp.2020.103766

Conflict of Interest: LL, QL, and XL were employed by the Engineering Research Institute of Appraisal and Strengthening of Shandong Jianzhu University Co., LTD. JY, GL, and ZL were employed by the Shandong Luqiao Group Co., Ltd.

Publisher's Note: All claims expressed in this article are solely those of the authors and do not necessarily represent those of their affiliated organizations, or those of the publisher, the editors, and the reviewers. Any product that may be evaluated in this article, or claim that may be made by its manufacturer, is not guaranteed or endorsed by the publisher.